Bulletin of the Seismological Society of America, Vol. 87, No. 3, pp. 606–619, June 1997

Regional *Lg* Attenuation for the Continental United States

by Harley M. Benz, Arthur Frankel, and David M. Boore

Abstract Measurements of the Fourier amplitude spectra of *Lg* phases recorded at high frequency (0.5 to 14.0 Hz) by broadband seismic stations are used to determine regional attenuation relationships for southern California, the Basin and Range Province, the central United States, and the northeastern United States and southeastern Canada. Fourier spectral amplitudes were measured every quarter octave from *Lg* phases windowed between 3.0 and 3.7 km sec^{-1} and recorded in the distance range of 150 to 1000 km. Attenuation at each frequency is determined by assuming a geometrical spreading exponent of 0.5 and inverting for Q and source and receiver terms. Both southern California and the Basin and Range Province are well described by low *Lg* Q and frequency-dependent attenuation. *Lg* spectral amplitudes in southern California are fit at low frequencies (0.625 to 0.875 Hz) by a constant *Lg* Q of 224 and by a frequency-dependent *Lg* Q function $Q = 187^{+7}_{-7} f^{0.55(\pm 0.03)}$ in the frequency band 1.0 to 7.0 Hz. The Basin and Range Province is characterized by a constant *Lg* Q of 192 for frequencies of 0.5 to 0.875 Hz and by the frequency-dependent *Lg* Q function $Q = 235^{+11}_{-11} f^{0.56(\pm 0.04)}$ in the frequency band 1.0 to 5.0 Hz. A change in frequency dependence above 5.0 Hz is possible due to contamination of the *Lg* window by *Pn* and *Sn* phases. *Lg* spectral amplitudes in the central United States are fit by a mean frequency-independent *Lg* Q of 1291 for frequencies of 1.5 to 7.0 Hz, while a frequency-dependent *Lg* Q of $Q = 1052^{+91}_{-83}(f/1.5)^{0.22(\pm 0.06)}$ fits the *Lg* spectral amplitudes for the northeastern United States and southeastern Canada over the passband 1.5 to 14.0 Hz. Attenuation measurements for these areas were restricted to frequencies >1.5 Hz due to larger microseismic noise levels at the lower frequencies.

Introduction

It has been well documented from felt intensities and instrumental seismic recordings that areas of active tectonics, like the western United States, have higher attenuation than the stable craton of the eastern United States (Nuttli *et al.,* 1979; Aki, 1980; Singh and Herrmann, 1983). Possible mechanisms to explain these observations are a highly fractured crust in tectonically active regions that effectively absorb high-frequency seismic waves (Aki, 1980), differences in crustal temperature (Frankel, 1991), and variations in crustal structures that control elastic wave propagation (Gregersen, 1984). In this article, we compare high-frequency *Lg* attenuation for southern California, the Basin and Range Province, and portions of the central and eastern United States, each region characterized by a different tectonic history and crustal properties. Both the Basin and Range Province and southern California are characterized by high heat flow (~1.5 HFU), high elevations (>500 m), thin crust (<40 km thick), and active Quaternary tectonics that have produced M 7+ earthquakes in recent decades, while the central and northeastern United States exhibit average continent heat flow (~1 HFU), thick continental crust (>40 km thick), and moderate earthquake activity with low recurrence rates for large events. This study provides an assessment of the differences in *Lg* attenuation between each region and constraints on high-frequency attenuation in the crust.

Observed as the dominant phase at regional distances, the *Lg* phase propagates as a higher-order, crustal-guided surface wave (Knopoff *et al.,* 1973); consequently, it provides the best measure of path-averaged crustal properties such as crustal *S*-wave velocity and attenuation. Because *Lg* is generally the largest high-frequency phase in regional seismic waveforms, it is used extensively to determine a wide variety of effects that include earthquake-source parameters, site response, and attenuation (Atkinson and Mereu, 1992).

Numerous studies have determined frequency-dependent *Lg* attenuation for the continental crust (Nuttli, 1973; Chavez and Priestley, 1986; Hasegawa, 1985; Atkinson and Mereu, 1992). Often the frequency-dependent quality factor Q is modeled using a power law of the form

$$Q(f) = Q_0(f/f_0)^{\eta}, \tag{1}$$

where f_0 is a reference frequency, Q_0 is Q at the reference frequency, and η is assumed constant over the frequencies of interest. For the Basin and Range Province, several *Lg* attenuation studies (Chavez and Priestley, 1986; Nuttli, 1986; Xie and Mitchell, 1990) have documented a strong frequency-dependent attenuation with Q_0 values of 139 to 267 and η between 0.37 and 0.6. Numerous *Lg* attenuation studies in the northeastern United States and southeastern Canada find a weaker frequency dependency and lower attenuation with Q_0 ranging from 561 to 1100, η between 0.19 and 0.45 (Hasegawa, 1985; Chun *et al.*, 1987; Gupta and McLaughlin, 1987; Atkinson and Mereu, 1992; Shi *et al.*, 1996). From regionalization of crustal coda-Q results, Singh and Herrmann (1983) find southern California and Basin and Range Province Q_0 values of 150 to 320 and η ranging from 0.4 to 0.6. For the central United States, they find Q_0 varying from 900 to 1350 with a frequency dependence described by η values of 0.1 to 0.3. In their study, the northeastern United States has intermediate values of η in the range 0.3 to 0.4 and Q_0 ranging from 780 to 900. However, theoretical studies indicate that coda Q may not equal shear-wave Q in strongly scattering media (Frankel and Wennerberg, 1987).

The *Lg* waveform data used in this study were obtained from local and regional earthquakes recorded by three-component broadband stations of the Berkeley Digital Seismic Network (BDSN) in northern California, Canadian National Seismograph Network (CNSN), Incorporated Research Institutions in Seismology (IRIS), Terrascope in southern California, United States National Seismograph Network (USNSN), and other cooperative stations. Figure 1 shows the velocity response of the north component of several of the sensors used in this study. The availability of high-quality, calibrated waveforms from different regions of the United States and Canada allows for consistent processing and interpretation of the *Lg* attenuation results. Table 1 lists the locations of the broadband stations used in this study. Unless otherwise noted, attenuation referred to in this article does not distinguish between intrinsic and scattering attenuation but represents an apparent attenuation for the whole crust.

We restricted our study in southern California and the central United States to frequencies less than 7 Hz because most stations were sampled at 20 samples/sec, using a flat antialiasing filter response to 7 Hz. For the Basin and Range Province and the northeastern United States and southeastern Canada, attenuation was measured up to 14 Hz, since most of the stations were sampled at 40 samples/sec or greater.

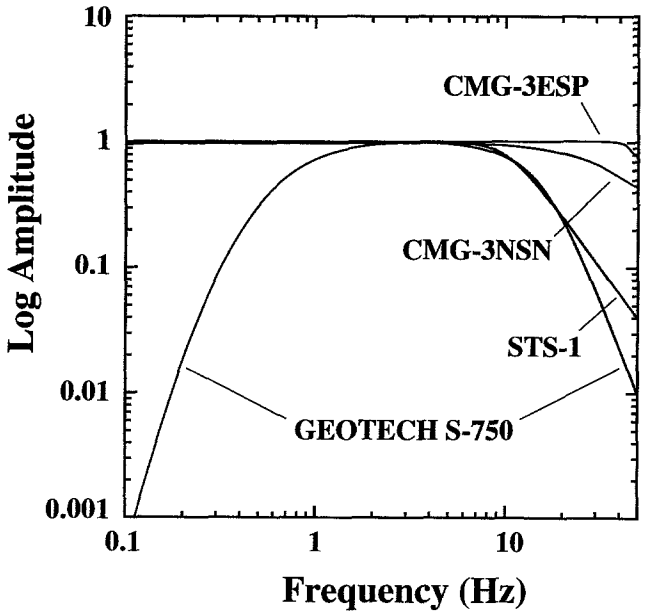

Figure 1. Amplitude response curves of the north component for several of the broadband sensors used in this study.

Measurements of *Lg* Spectral Amplitudes

The basic formula describing the spectral amplitude A_{ij} at frequency f for the ith station and jth earthquake is

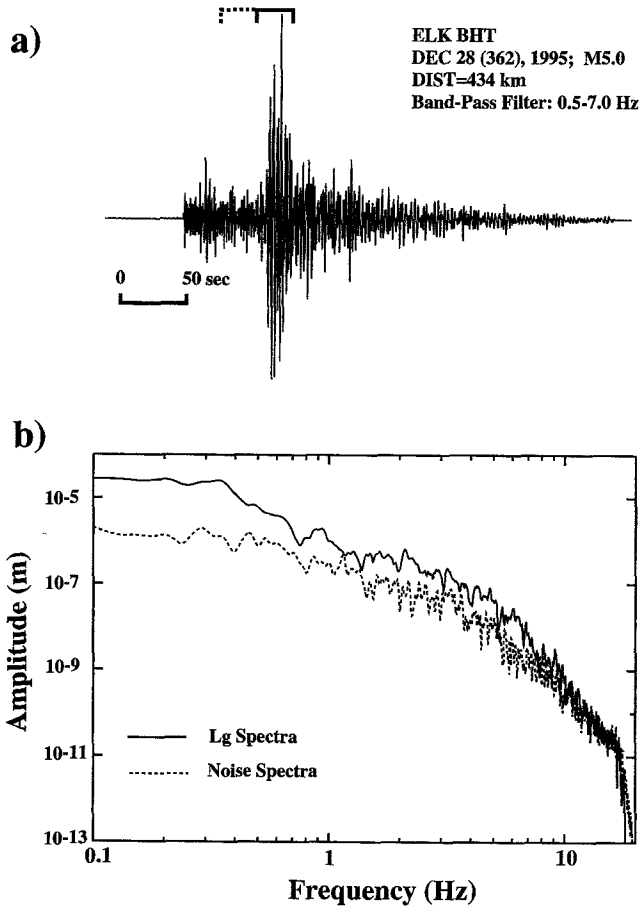

Figure 2. Example of a transverse-component broadband waveform used in this study. The transverse-component broadband waveform (a) shows the *Lg* (solid) and noise (dashed) windows, while (b) shows a comparison of the *Lg* and noise spectra of the windowed data.

Table 1
Locations of the Broadband Stations Used in This Study

Station Name	Latitude	Longitude	Elev (m)	Study Region
BINY	42.199N	75.986W	498	NE U.S. and SE Canada
CBM	46.933N	68.120W	250	NE U.S. and SE Canada
GAC	45.703N	75.478W	62	NE U.S. and SE Canada
HRV	42.506N	71.558W	180	NE U.S. and SE Canada
LBNH	44.240N	71.926W	367	NE U.S. and SE Canada
LMN	45.852N	64.806W	363	NE U.S. and SE Canada
LMQ	47.548N	70.327W	419	NE U.S. and SE Canada
LSCT	41.678N	73.224W	318	NE U.S. and SE Canada
RSNY	44.548N	74.530W	396	NE U.S. and SE Canada
SADO	44.769N	79.142W	243	NE U.S. and SE Canada
YSNY	42.476N	78.538W	628	NE U.S. and SE Canada
CCM	38.060N	91.240W	222	Central U.S.
GOCA	33.411N	83.467W	150	Central U.S.
MCWV	39.658N	79.846W	280	Central U.S.
MIAR	34.546N	93.573W	207	Central U.S.
MYNC	35.074N	84.128W	550	Central U.S.
OXF	34.512N	89.409W	101	Central U.S.
WMOK	34.738N	98.781W	486	Central U.S.
BMN	40.431N	117.221W	1500	Basin and Range
DUG	40.195N	112.813W	1477	Basin and Range
ELK	40.744N	115.240W	2210	Basin and Range
GSC	35.303N	116.806W	990	Basin and Range
KNB	37.017N	112.822W	1715	Basin and Range
LAC	34.389N	116.411W	793	Basin and Range
MLAC	37.630N	118.836W	2134	Basin and Range
MNV	38.433N	118.153W	1524	Basin and Range
NEE	34.824N	114.599W	139	Basin and Range
TPNV	36.929N	116.224W	1600	Basin and Range
WVOR	42.434N	118.637W	1344	Basin and Range
BAR	32.680N	116.672W	496	Southern California
BKS	37.877N	122.235W	276	Southern California
CALB	34.140N	118.628W	276	Southern California
CMB	38.035N	120.385W	719	Southern California
DGR	33.650N	117.009W	609	Southern California
GLA	33.051N	114.828W	514	Southern California
GSC	35.302N	116.806W	954	Southern California
ISA	35.663N	118.474W	817	Southern California
JRSC	37.404N	122.240W	103	Southern California
MHC	37.342N	121.642W	1282	Southern California
MLAC	37.630N	118.836W	2134	Southern California
PKD1	35.889N	120.425W	466	Southern California
PAS	34.148N	118.171W	257	Southern California
PFO	33.612N	116.459W	1245	Southern California
RPV	33.743N	118.404W	64	Southern California
SAO	36.765N	121.445W	350	Southern California
SBC	34.441N	119.715W	61	Southern California
SMTC	32.949N	115.720W	3	Southern California
STAN	37.404N	122.174W	159	Southern California
SVD	34.106N	117.098W	574	Southern California
USC	34.019N	118.286W	17	Southern California
VTV	34.561N	117.330W	812	Southern California

$$A_{ij}(f) = R_{ij}^{-\gamma} S_j(f) G_i(f) e^{-\pi f R_{ij}/Q\beta}, \quad (2)$$

where $S_j(f)$ is the source spectra, $G_i(f)$ is the site amplification, R_{ij} is the distance between the earthquake and the station, γ is the exponent for geometrical spreading, and β is the average S-wave velocity for the crust. Taking the logarithm of both sides of (2) results in the following equation:

$$\ln A_{ij}(f) + \gamma \ln R_{ij} = \ln G_i(f) + \ln S_j(f) - \pi f R_{ij}/Q\beta. \quad (3)$$

By measuring the Lg amplitude at a single frequency f, we

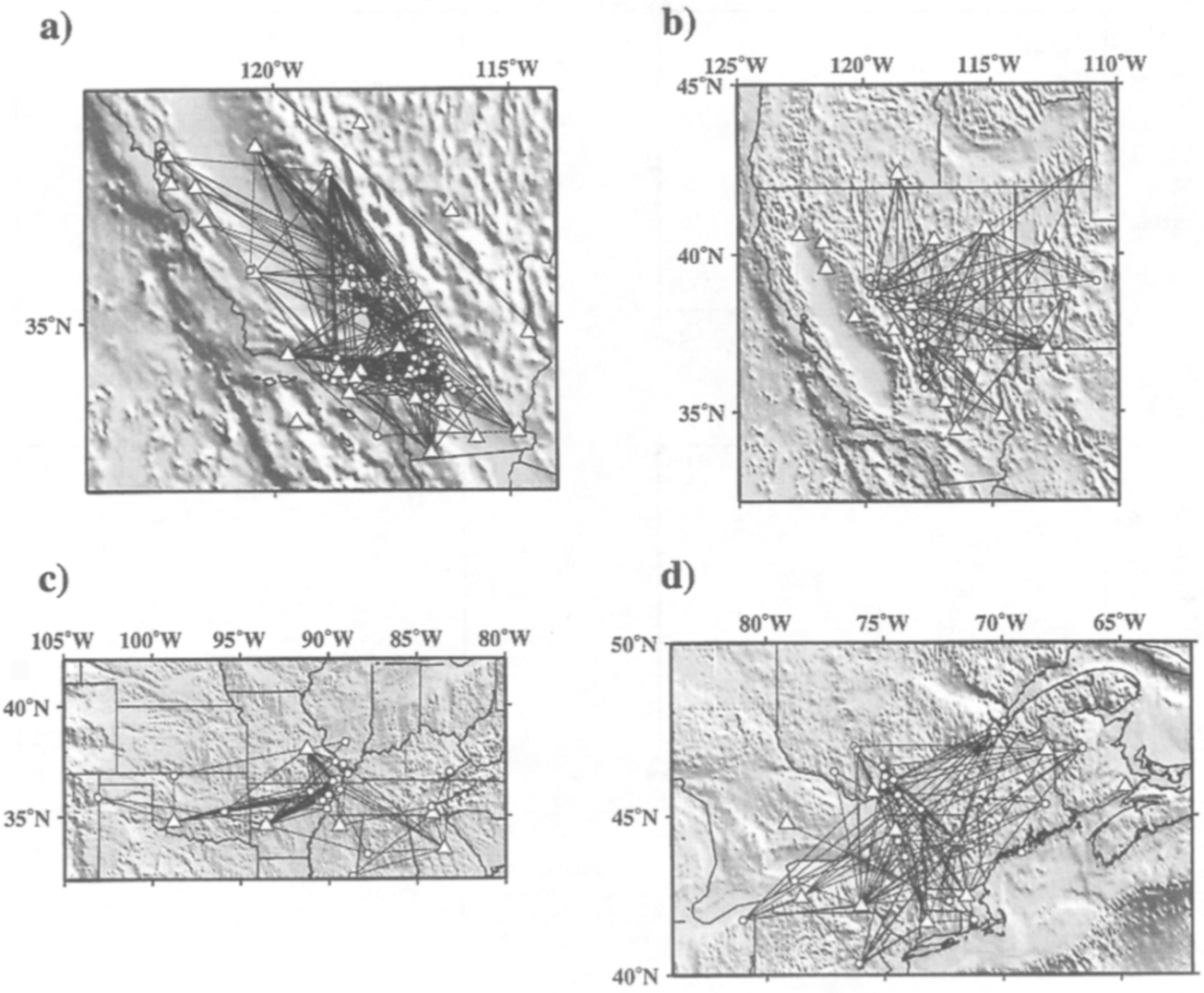

Figure 3. Maps of (a) southern California, (b) the Basin and Range Province, (c) the central United States, and (d) northeastern United States and southeastern Canada showing the regions sampled in this study. Triangles represent broadband stations in the study region, while small circles are the earthquakes used in the study. Lines represent earthquake and station pairs for which there is an *Lg* spectral measurement at 3 Hz.

can invert for the source (S_j) and receiver (G_i) terms and *Lg* *Q*, assuming a fixed geometrical spreading term γ and average crustal *S*-wave velocity. An average crustal shear velocity of 3.5 km sec^{-1} was assumed for each of the study regions, which is within the velocity window from 3.0 to 3.7 km sec^{-1} that is used to define the *Lg* phase (Fig. 2). Visual inspection of all the *Lg* phases used in this study showed that the peak amplitude lies within this window. Varying the *Lg* window length used to define the *Lg* phase had negligible effects on the results. The radiation pattern of the source is not considered in this formulation since we assume that it has minimal effect on the spectral measurements at high frequencies, and any such effect would tend to average out over multiple events and paths. In addition, Castro *et al.* (1990) show that the estimation of *Q* is not strongly effected by the radiation pattern. Results will also confirm this assumption. By solving for *Lg* *Q* at a single frequency, the effects of the source corner frequency are accounted for in the source term, *Sj*. The inversion is constrained by assuming one station has a unit receiver term and all other receiver terms are relative to the constraining station. Results will show that the selection of the reference station has little influence on the determination of *Lg* *Q*.

It is difficult to simultaneously estimate geometrical spreading and attenuation; consequently, we assume a frequency-independent geometrical spreading function with $\gamma = 0.5$ for each region. Synthetic *Lg* simulations by Herrmann and Kijko (1983) assuming a simple plane-layered velocity structure shows that the *Lg* spectral amplitudes behave as cylindrical waves with an $r^{-0.5}$ fall-off, while Bowman

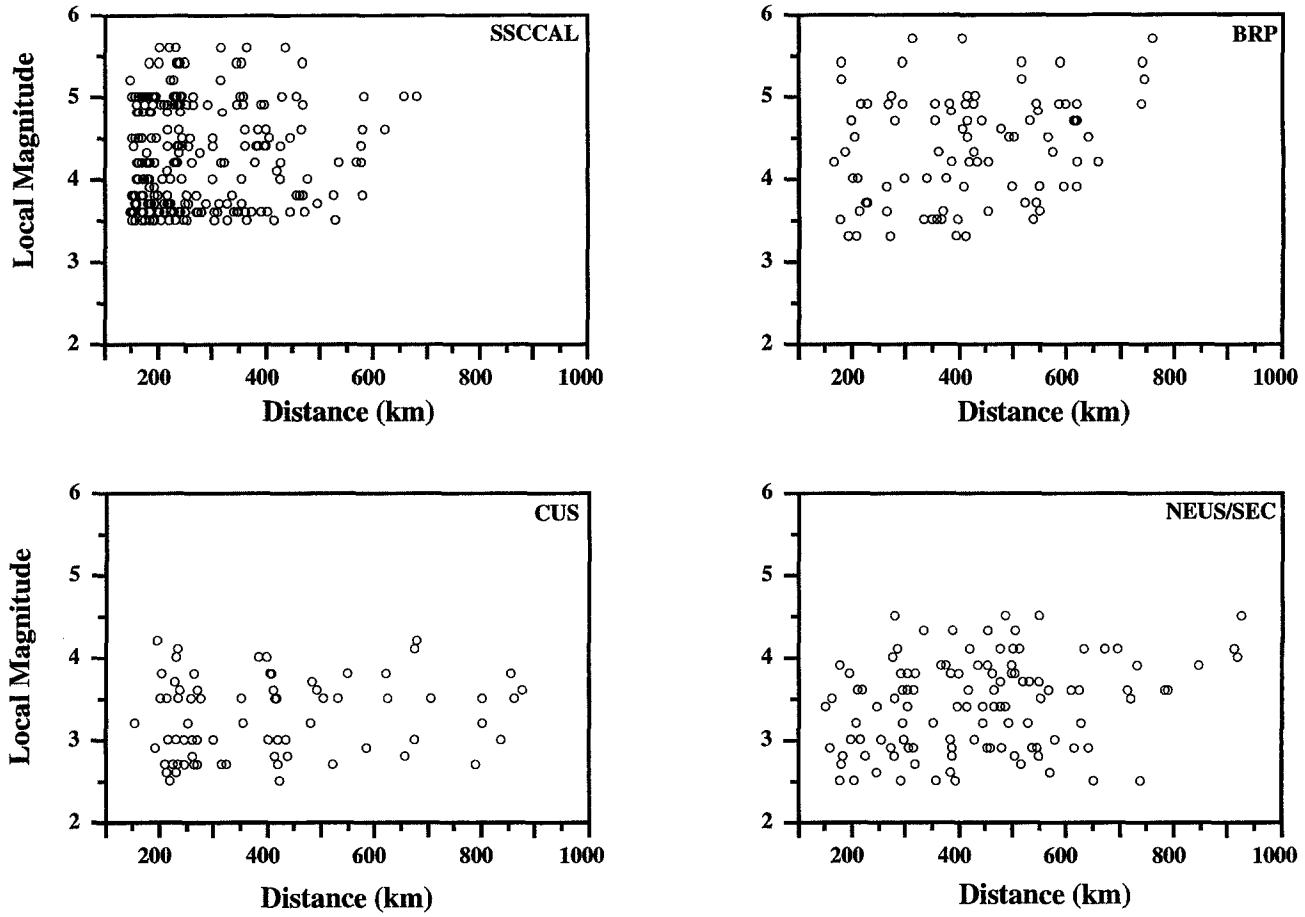

Figure 4. Distribution of observed *Lg* spectral amplitudes at 3 Hz as a function of local earthquake magnitude and distance for the four study regions, which are: southern and south-central California (SSCCAL), the Basin and Range Province (BRP), the central United States (CUS), and the northeastern United States and southeastern Canada (NEUS/SEC).

and Kennett (1991) show that the coefficient of geometrical spreading is sensitive to velocity gradients in the crust. Because we are investigating *Lg* attenuation for different regions that have different crustal structures and compositions, it is beyond the scope of this article and the available data to determine the coefficient of geometrical spreading for each region.

Weighted least-squares regression analysis is used to fit frequency-dependent functions to the Q observations (equation 1) for each region. The functional form $Q = Q_0(f/f_0)^{\eta}$ is transformed by taking the logarithm of both sides, resulting in the following equation:

$$\ln Q = \ln Q_0 + \eta * \ln (f/f_0), \qquad (4)$$

where $\ln Q_0$ and η are the unknowns to be determined. The estimated uncertainties, based on formal regression analysis, are for the unknown parameters $\ln Q_0$ and η, which results in asymmetric error bounds on Q_0. It should be kept in mind that there is a strong negative correlation between $\ln Q_0$ and η. A bootstrap-with-replacement analysis of the fit to the data for southern California shows that the confidence regions at standard probability levels can be approximated by narrow ellipses whose major axes have trends with negative slopes. The confidence limits on $\ln Q_0$ and η are consistent with the uncertainties provided by the formal regression analysis.

For our analysis, we selected earthquakes less than 18 km deep that were recorded in the distance range of 150 to 1000 km by two or more stations. Requiring two or more observations per earthquake helps reduce the trade-off between the source and receiver terms (equation 3). To measure *Lg* spectral decay, we first corrected the horizontal-component seismograms for instrument response and obtained ground displacement; we then rotated them to produce radial and transverse-component seismograms. The *Lg* phase was then defined by the velocity window 3.0 to 3.7 km sec^{-1} on the transverse-component–displacement seismograms. McNamara *et al.* (1996) found for a similar frequency range that the *Lg* phases propagating across the Tibetan plateau exhibited more consistent energy on the transverse component than on the radial or horizontal components. The Fourier spectra of windows containing *Lg* ground displacement

and a noise sample of comparable length were then computed and smoothed using a 5-point running average. *Lg* spectral amplitudes were measured every quarter octave between 0.5 and 7.0 Hz for instruments sampled at 20 samples/sec and between 0.5 and 14.0 Hz for instruments sampled at 40 samples/sec or greater. Only values with a signal-to-noise ratio greater than 2 were used in the analysis. Figure 2 shows an example of a transverse-component seismogram and the *Lg* and noise windows. The noise window used in this study (Fig. 2), which is the same length in time as the *Lg* window and immediately precedes the *Lg* window, is considered a conservative estimate of noise since it contains ambient ground noise and *P*- and *S*-wave coda, each of which can contaminate the *Lg* phase.

Regional Attenuation Measurements

Figures 3a through 3d show the distribution of broadband stations, earthquakes, and *Lg* paths for the four regions investigated. Lines connecting earthquakes and stations represent earthquake-station pairs used in the analysis of *Lg* attenuation at 3 Hz for each of the study regions. The maps were constructed at 3 Hz because this frequency represents the portion of the frequency band of interest with the best signal-to-noise ratio, thus providing a view of crustal sampling in each study region. Southern and south-central California, which includes the southern Coast Ranges and southern Sierra Nevada, is covered by 230 raypaths from 45 earthquakes recorded at 22 stations. Excluded are the eastern Mojave and extensional regions east of the Sierra Nevada. In addition, the station on San Nicholas Island off the west coast of southern California was not used because it was relatively noisy and there were comparative few spectral measurements from the station. Broadband stations in the Basin and Range are not used in order to eliminate propagation paths through the southern Basin and Range Province. The focus in southern California is to characterize the regional attenuation for areas affected by seismicity along the San Andreas and Garlock fault systems and to compare the results with extensional environments like the Basin and Range Province. The Basin and Range Province is sampled by 90 raypaths from 30 earthquakes recorded by 11 stations (Fig. 3b). Most of the west-central Basin and Range Province is covered, but the eastern Basin and Range Province is poorly sampled due to fewer stations and earthquakes. California broadband stations west of the Sierra Nevada are not used in order to eliminate sampling of the Sierra Nevada batholith, a Mesozoic feature relatively undeformed by Basin and Range Province type Quaternary deformation.

Fewer observations are available for the eastern United States, primarily due to lower rates of seismicity, few broadband stations, and the brief period of available broadband recordings (since about 1992). Earthquakes in the central United States are primarily located in the New Madrid Seismic Zone (NMSZ), which restricts good areal distribution of raypaths (Fig. 3c). The majority of the 73 raypaths from 30

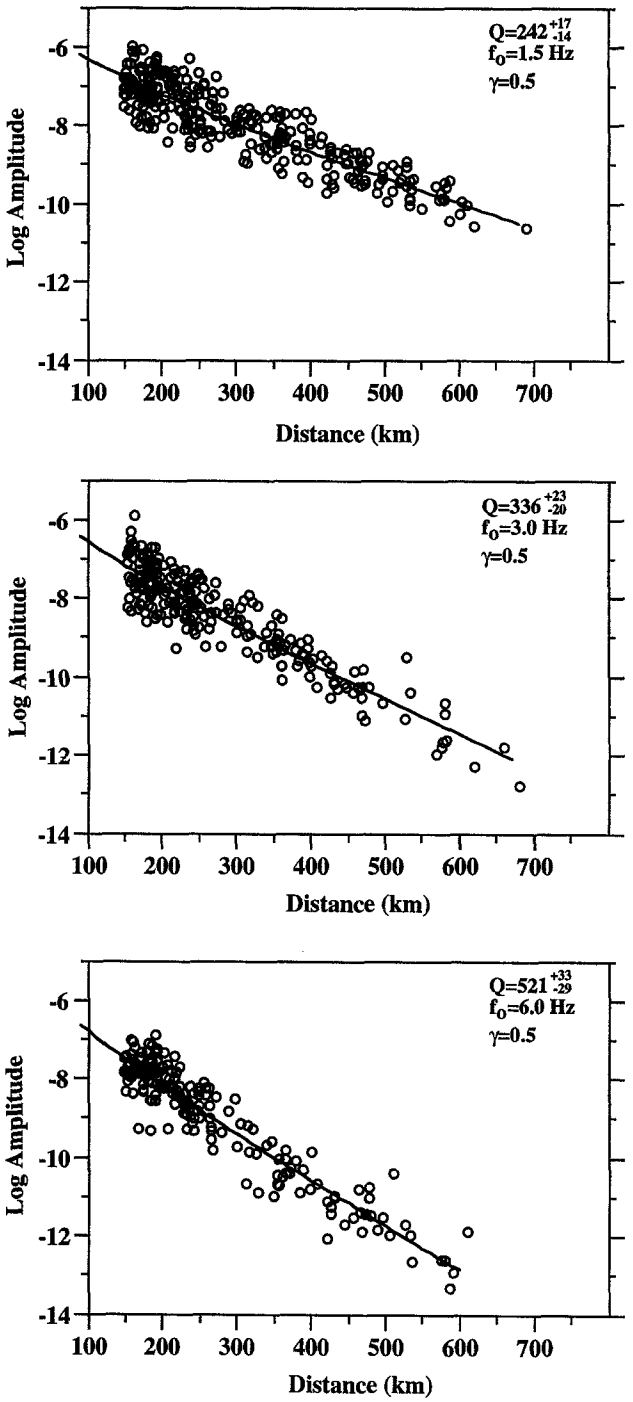

Figure 5. *Lg* spectral amplitudes (circles) in southern and south-central California at 1.5, 3.0, and 6.0 Hz, corrected for source and receiver terms (see equation 3). The solid curve is the best-fit to the observed data assuming frequency-independent *Lg Q* and a γ of 0.5.

earthquakes are recorded at three of the seven stations in the central United States. The northeastern United States and southeastern Canada are sampled by 116 raypaths from 31 earthquakes recorded at 10 stations (Fig. 3d). The distribution of earthquakes and stations shows that sampling of the

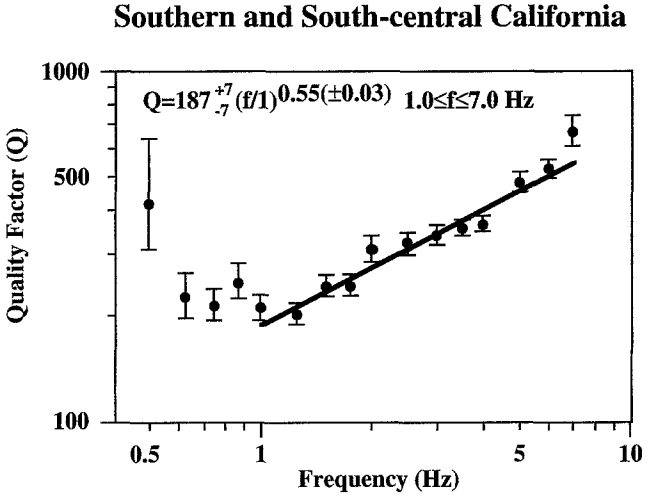

Figure 6. Values of *Lg Q* in southern and south-central California determined by inversion of the *Lg* spectral amplitudes at quarter-octave frequencies between 0.5 and 7.0 Hz, assuming frequency-independent *Lg Q* at each frequency and a γ of 0.5. Best-fit frequency-dependent *Lg Q* function is $Q = 187^{+7}_{-7}(f/1)^{0.55(\pm 0.03)}$ between 1.0 and 7.0 Hz.

crust is relatively uniform for northeastern United States and southeastern Canada due to the diffuse seismicity throughout the region. While there are fewer spectral measurements for the eastern study areas, compared to the southern California and the Basin and Range Province, the data are sufficient for accurately determining regional attenuation.

Shown in Figure 4 are plots of the earthquake magnitude versus distance for the four study regions obtained from spectral observations at 3 Hz. Both the Basin and Range Province and southern and south-central California are represented by higher mean magnitudes, resulting in a better overall signal-to-noise ratio. Southern California observations were restricted to *M* 3.5 or greater since smaller-magnitude events provided good signal to noise only to 300 to 400 km at high frequency. The maximum observable distance of about 700 km was due to the limited aperture of the network (Fig. 3a). For the Basin and Range, *M* 3.0 was found to be a lower limit in order to obtain good observations at distances greater than about 400 km and recordings at two or more stations. For the eastern United States, there is a good distribution of earthquakes over approximately two magnitude units and distances of 150 to 900 km. *M* 2.5 was the practical lower limit for earthquake in the east to be well recorded by two or more stations at distances greater than

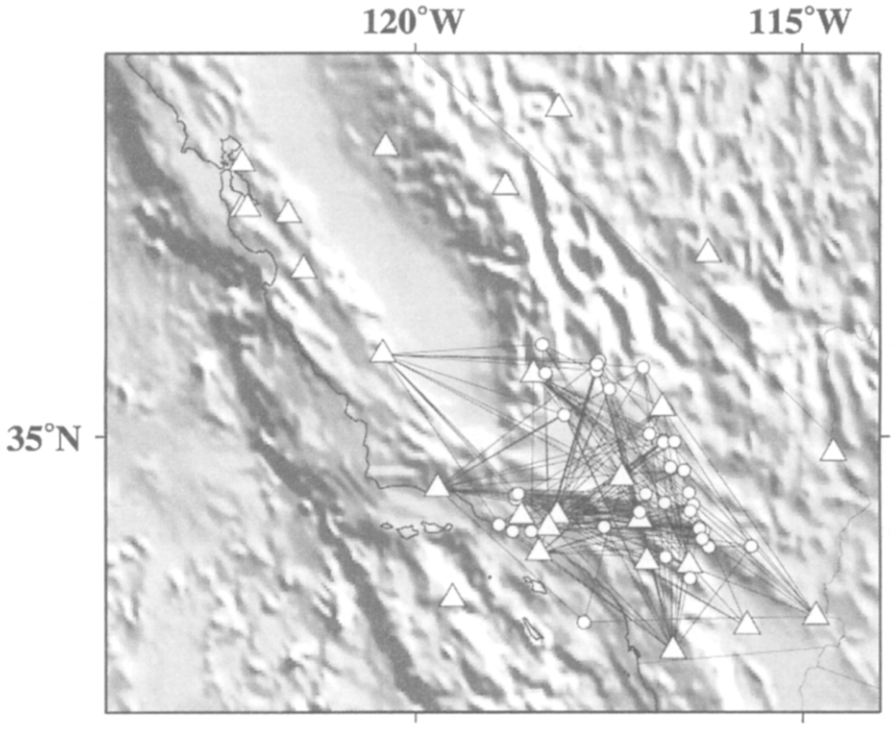

Figure 7. Map of southern and central California showing the regions sampled when using only broadband stations in southern California. Triangles represent broadband stations in the study region, while small circles are the earthquakes used in the study. Lines represent earthquake and station pairs for which there is an *Lg* spectral measurement at 3 Hz.

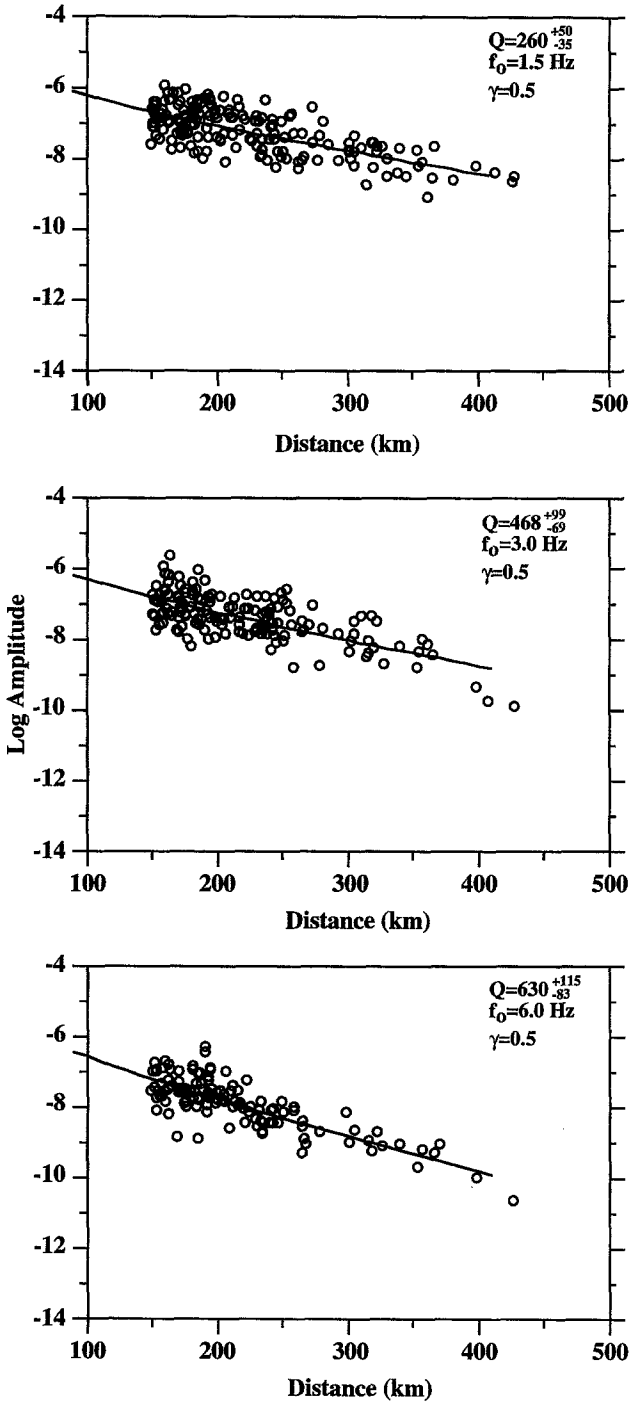

Figure 8. *Lg* spectral amplitudes (circles) at 1.5, 3.0, and 6.0 Hz using only southern California broadband stations, corrected for source and receiver terms (see equation 3). The solid curve is the best-fit to the observed data assuming frequency-independent Q and a γ of 0.5.

150 km. Magnitudes and locations for the western United States earthquakes were taken from the regional network when available, all other earthquake magnitudes and locations were taken from the Preliminary Determination of Epicenters (PDE).

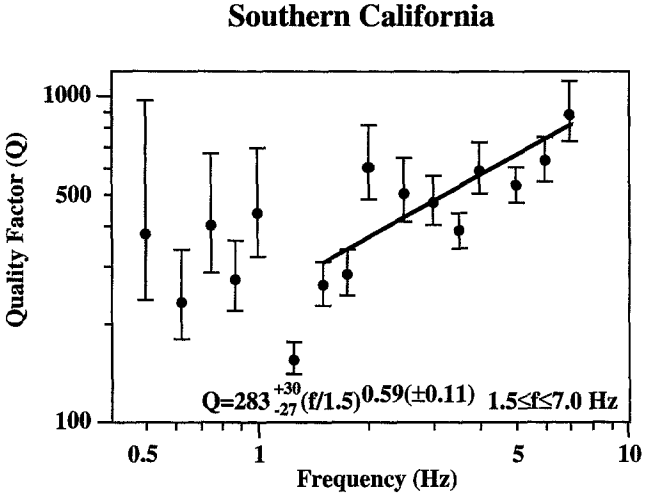

Figure 9. Values of *Lg* Q in southern California determined by inversion of the *Lg* spectral amplitudes using only southern California broadband stations measured every quarter-octave frequencies between 0.5 and 7.0 Hz, assuming frequency-independent Lg Q at each frequency and a γ of 0.5. Best-fit frequency-dependent *Lg* Q function is $Q = 283^{+30}_{-27}(f/1.5)^{0.59(\pm 0.11)}$ between 1.5 and 7.0 Hz.

Southern and South-Central California

Figure 5 shows a comparison of the *Lg* spectral amplitudes at frequencies of 1.5, 3.0, and 6.0 Hz, corrected for source and receiver terms determined from the inversion, and the best-fit curve to the data at each frequency. Station ISA, located on the edge of the southern Sierra Nevada mountains, is used as the reference station. Results show an increase in *Lg* Q from 242^{+17}_{-14} at 1.5 Hz to 521^{+33}_{-29} at 6.0 Hz. The error terms, denoted by the plus and minus values, are derived from the formal uncertainties in the estimate of Q^{-1}, resulting in the asymmetric error bounds on *Lg* Q. Overall, the scatter in spectral amplitudes decreases with increasing frequency. This is possibly due to stronger effects of radiation pattern at lower frequencies, which is not corrected for in the inversion, and a general increase in the microseismic noise at lower frequencies. Results show that the *Lg* Q is well determined over more than three octaves between 0.5 and 7.0 Hz. Performing 22 separate inversions for *Lg* Q at 3 Hz, using each of the 22 stations as a reference station in turn, resulted in *Lg* Q varying from 334 to 340, which indicates that the determination of *Lg* Q is not sensitive to the reference station. Selection of the reference station is most important when interpreting relative receiver terms, which is not discussed in this article.

Plotting *Lg* Q as a function of frequency (Fig. 6) shows that for frequencies less than 1.0 Hz, the estimated *Lg* Q has larger errors and is not noticeably frequency dependent with a mean *Lg* Q of 224, provided the Q estimate at 0.5 Hz is excluded, which has significantly larger errors than the other Q estimates. For frequencies between 1.0 and 7.0 Hz, *Lg* Q

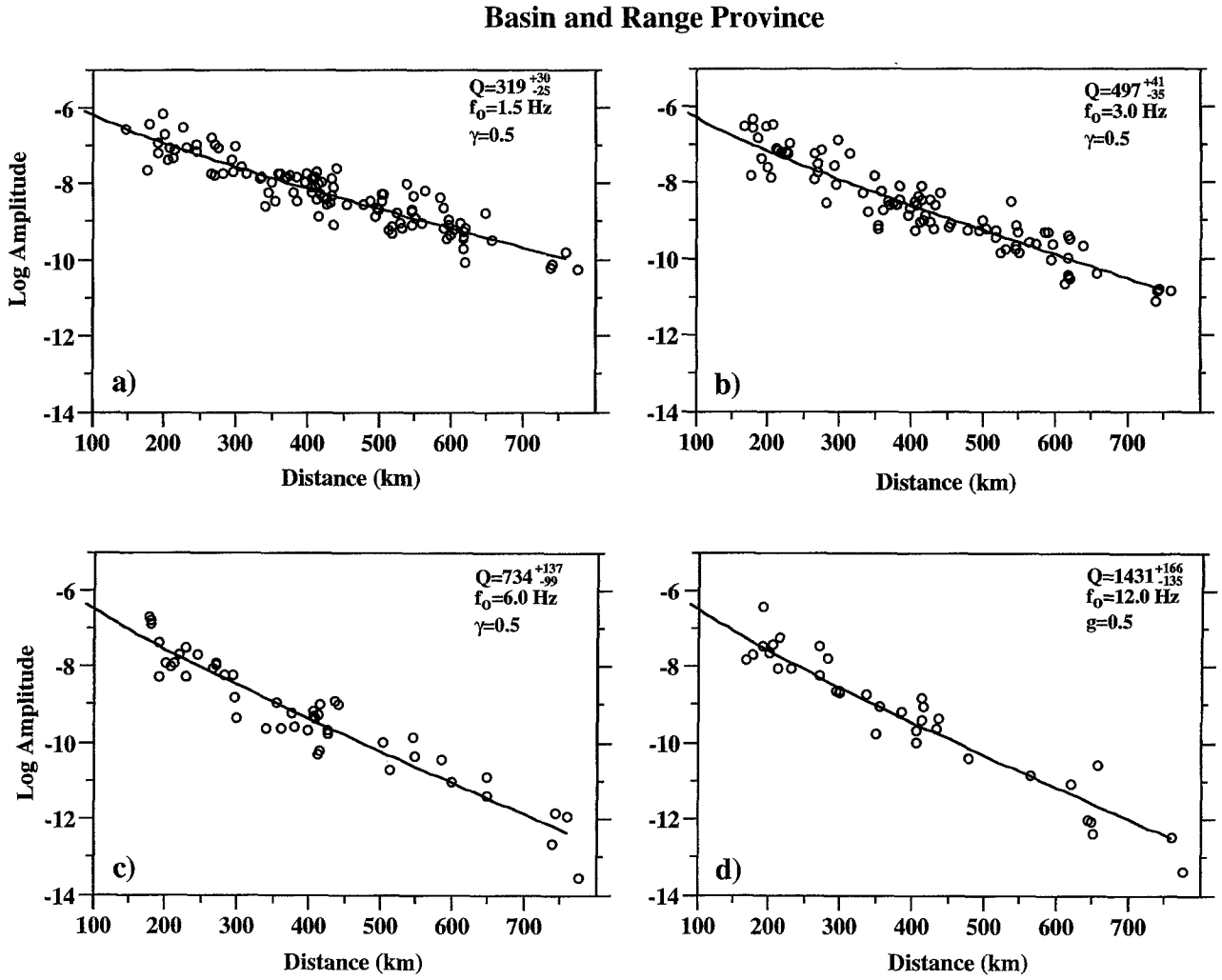

Figure 10. *Lg* spectral amplitudes (circles) for the Basin and Range Province at 1.5, 3.0, 6.0, and 12.0 Hz, corrected for source and receiver terms (see equation 3). The solid curve is the best-fit to the observed data assuming frequency-independent *Lg Q* and a γ of 0.5

increases from 210^{+19}_{-16} at 1.0 Hz to 666^{+75}_{-61} at 7 Hz. Fitting the *Lg Q* estimates (Fig. 6) in this frequency range with a frequency-dependent attenuation function of the form described in equation (1) results in the best-fit function $Q = 187^{+7}_{-7}(f/1)^{0.55(\pm 0.03)}$. This Q function is comparable to previously determined attenuation functions for the Basin and Range Province, where Q_0 varies from 139 to 214, η ranges from 0.5 to 0.6, and $\gamma = 0.5$ (Chavez and Priestley, 1986; Nuttli, 1986). This is also consistent with the crustal coda-Q results of Singh and Herrmann (1983) who find an average Q_0 of 200 and η of 0.6 for southern California.

To understand the influence of central California stations on the results, we inverted for *Lg Q* using only stations in southern California. Figure 7 shows the raypath coverage for *Lg* measurements at 3 Hz using only southern California stations. These data no longer contain information on paths along the eastern Sierra Nevada and southern Coast Ranges. *Lg* spectral amplitudes for frequencies 1.5, 3.0, and 6.0 Hz show a larger degree of scatter than the previous results (Fig. 8), but the general trend of increasing *Lg Q* with frequency was maintained for the frequency band 1.0 to 7.0 Hz. Fitting a frequency-dependent attenuation function between 1.5 and 7.0 Hz (Fig. 9), over which a frequency dependence is observed, results in the function $Q = 283^{+30}_{-27}(f/1.5)^{0.59(\pm 0.11)}$. In both cases, attenuation in southern California is described by low Q and a strong frequency dependence in the frequency range of 1.0 to 7.0 Hz.

Basin and Range Province

Shown in Figures 10a through 10d are the best-fit curves to the Basin and Range Province *Lg* spectral amplitudes, corrected for source and receiver terms, at frequencies of 1.5, 3.0, 6.0, and 12.0 Hz. MNV, located roughly in the middle of the network (see Table 1), is used as a reference site. Results show that *Lg Q* increases from 319^{+30}_{-25} at 1.5 Hz to 1431^{+166}_{-135} at 12.0 Hz and that the estimates of *Lg Q* are

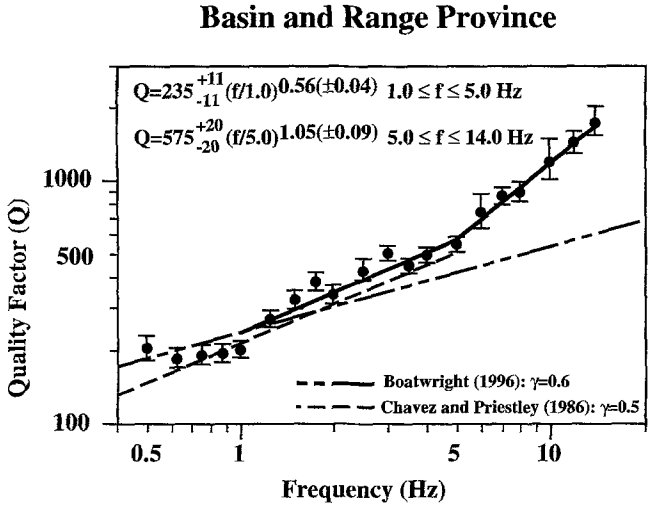

Figure 11. Values of *Lg Q* in the Basin and Range Province determined by inversion of the *Lg* spectral amplitudes measured every quarter-octave frequencies between 0.5 and 12.0 Hz, assuming frequency-independent *Q* at each frequency and a γ of 0.5. Best-fit frequency-dependent *Lg Q* functions between 1.0 and 5.0 Hz and 5.0 and 14.0 Hz are $Q = 235^{+11}_{-11}(f/1)^{0.56(\pm 0.04)}$ and $Q = 575^{+11}_{-11}(f/5)^{1.05(\pm 0.09)}$, respectively. Shown for comparison are previously determined frequency-dependent *Lg Q* functions using *Lg* data from the Basin and Range Province.

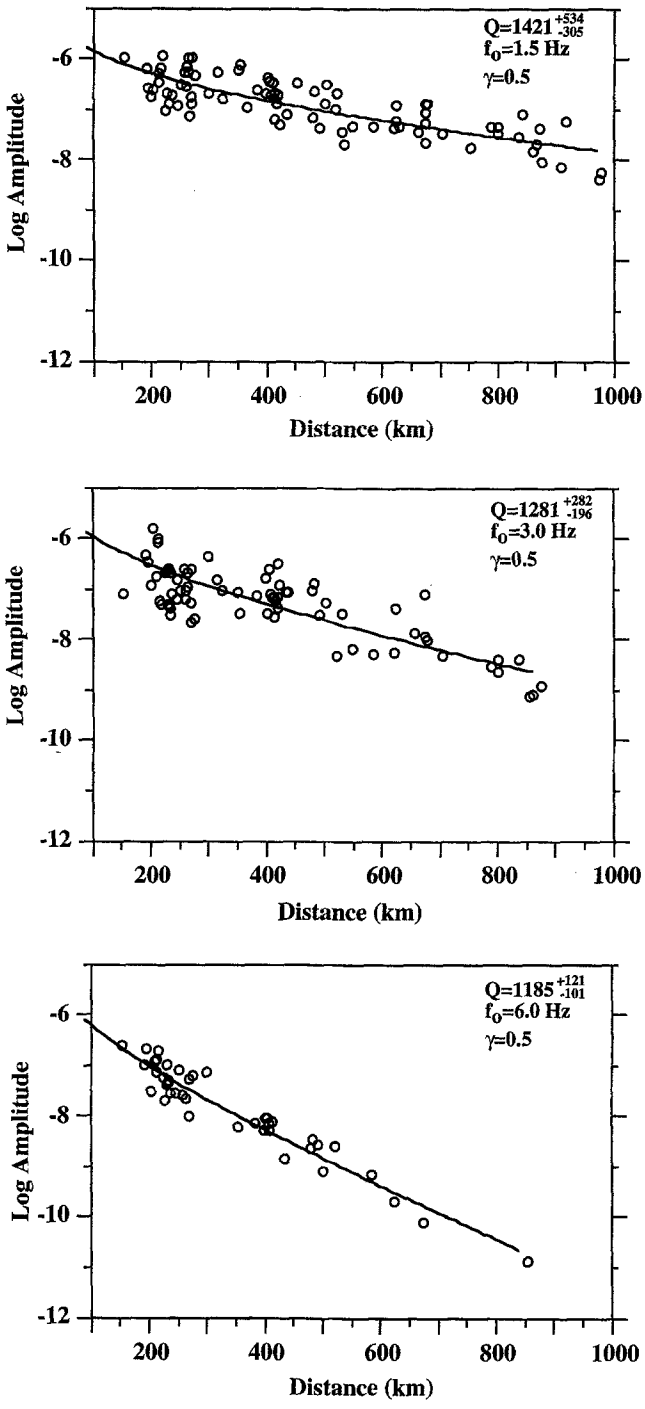

Figure 12. *Lg* spectral amplitudes (circles) for the central United States at 1.5, 3.0, and 6.0 Hz, corrected for source and receiver terms (see equation 3). The solid curve is the best-fit to the observed data assuming frequency-independent *Lg Q* and a γ of 0.5.

tightly constrained by the spectral observations. Like southern California, the Basin and Range Province results show a constant *Lg Q* for frequencies <1.0 Hz and a strong frequency dependence above 1.0 Hz (Fig. 11). The results (Fig. 11) also suggest that the frequency dependence changes above 5.0 Hz. For frequencies <1.0 Hz, *Lg Q* is characterized by a mean of 192. Fitting piecewise continuous *Q* functions for the frequency bands 1.0 to 5.0 Hz and 5.0 to 14.0 Hz results in the functions $Q = 235^{+11}_{-11}(f/1)^{0.56(\pm 0.04)}$ and $Q = 575^{+11}_{-11}(f/5)^{1.05(\pm 0.09)}$, respectively. The *Q* function from 1.0 to 5.0 Hz is close to that determined by Chavez and Priestley (1986) for a similar frequency range and comparable to an average Basin and Range crustal coda Q_0 of 300 and η of 0.4 (Singh and Herrmann, 1983). A recent attenuation study of the southern Basin and Range Province using *S*-wave data observed in the distance range 10 to 180 km (Boatwright, 1996) found a Q_0 of 238, η of 0.35, and γ of 0.6. A fit of our results with those of Boatwright (1996) found good agreement for frequencies less than about 5.0 Hz (Fig. 11). The *Lg* study of Brockman and Bollinger (1992) for the eastern Basin and Range in the vicinity of the Wasatch Front found a significantly lower Q_0 of 97 and a stronger frequency dependence with $\eta = 0.9$. It is difficult to compare our results directly with those of Brockman and Bollinger (1992), since the Wasatch Front region of central Utah is the least-sampled area in our study region, and they assumed a γ of 0.7 to 0.9. In all cases, the Basin and Range Province is defined by a strong frequency dependence with η in the range 0.35 to 0.6 and low Q_0.

Shin and Herrmann (1987) provide evidence that high-frequency (>7 Hz) *Sn* energy can interfere with the *Lg* phase, producing a change in *Lg* attenuation. An investiga-

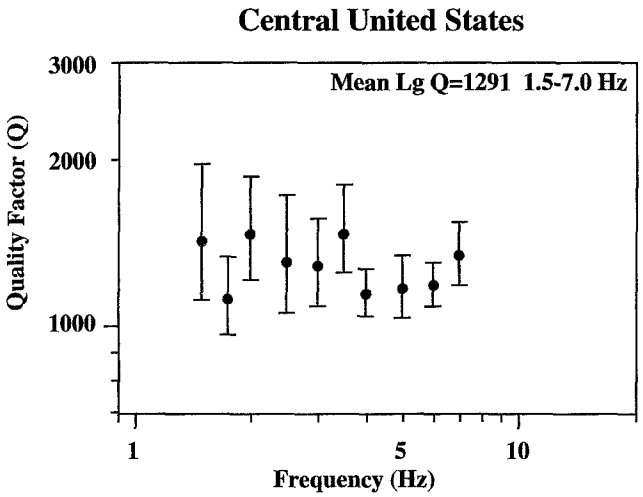

Figure 13. Values of *Lg Q* in the central United States determined by inversion of the *Lg* spectral amplitudes measured every quarter-octave frequencies between 1.5 and 7.0 Hz, assuming frequency-independent *Lg Q* at each frequency and a γ of 0.5. Results show no frequency-dependent *Lg Q* for the central United States. The mean *Lg Q* over the frequency range 1.5 to 7.0 Hz is 1291.

tion of our waveform data for distances greater than 450 km and at high frequencies (>5 Hz) shows that both *Pn* and *Sn* may contribute significant energy in the *Lg* window at frequencies above about 5.0 Hz. Consequently, we suggest that our Basin and Range *Lg Q* function in the frequency band 1.0 to 5.0 Hz is representative of *Lg* attenuation in the Basin and Range Province and that the *Q* function in the frequency band 5.0 to 14.0 Hz is showing the influence of additional phases.

Central United States

Due to the smaller number of available broadband recordings for earthquakes recorded by two or more stations and a poor signal-to-noise ratio at lower frequencies in the eastern study regions, there are insufficient spectral measurements to determine accurately *Lg Q* for frequencies less than about 1.5 Hz. Figure 12 shows that the spectral observations at 1.5, 3.0, and 6.0 Hz are well distributed over a distance range of 150 to 1000 km and that the estimated *Lg Q* at these frequencies is well constrained by the spectral observations. Shown in Figure 13 are the estimated *Lg Q* for the central United States over the frequency band 1.5 to 7.0 Hz. Results display considerable scatter over the frequencies of interest with *Lg Q* ranging from 1421^{+534}_{-305} at 1.5 Hz to 1341^{+199}_{-154} at 7.0 Hz. The present data set is insufficient to resolve a possible frequency dependence in *Lg Q* for the region; therefore, we describe the central United States by a frequency-independent *Lg Q* of 1291, based on averaging the observations between 1.5 and 7.0 Hz. These results are consistent with central United States crustal coda-*Q* observations of Singh and Herrmann (1983) who find Q_0 varies from 900 to 1350 at 1 Hz with a small frequency dependence described by η = 0.1 to 0.3.

Northeastern United States

Numerous attenuation studies have been conducted in the northeastern United States and southeastern Canada using a variety of wave types and methods for determining *Q*. The abundance of studies in this region is primarily due to the high-quality waveform data recorded by the Eastern Canadian Telemetry Network. Only in recent years has this network and seismic networks in the northeastern United States been augmented by broadband stations. Consequently, our study complements previous studies by extending the region of interest into the northeastern United States using standardized instrumentation across the whole region. A complete summary of previous studies is beyond our scope, but the reader is referred to Ebel (1994) who summarizes the different *Q* functions that have been determined for this region. We restrict a comparison of our results to those studies that used similar wave types, frequency bands, and assumptions on geometrical spreading. Consistent among all previous studies is that the region is best characterized by high *Q* and a weak frequency dependence (η typically less than 0.3).

For the frequencies 1.5, 3.0, 6.0, and 12.0 Hz, best-fit curves to the observed *Lg* spectral amplitudes are shown in Figure 14 to be well constrained over the distance range 150 to 700 km. The inverted *Lg Q* results for the northeastern United States and southeastern Canada show considerable scatter over the frequency range of 1.5 to 14.0 Hz (Fig. 15) but with a noticeable increase in *Lg Q* with frequency. *Lg Q* varies from a low of 970^{+148}_{-114} at 2.0 Hz to 1956^{+398}_{-282} at 14.0 Hz. A best-fit frequency-dependent *Q* function results in the function $Q = 1052^{+91}_{-83}(f/1.5)^{0.22(\pm 0.06)}$ over the frequency band 1.5 to 14.0 Hz (Fig. 15). This result is consistent with previous *Lg* attenuation studies in southeastern Canada (Hasegawa, 1985; Chun *et al.*, 1987; Atkinson and Mereu, 1992) that find Q_0 values of 670 to 1100, η between 0.19 and 0.33, and γ = 0.5. In fact, our results are bounded by the results of Hasegawa (1985) and Chun *et al.* (1987), with η only ranging from 0.19 to 0.22 between studies. *Lg Q* results of Shi *et al.* (1996) are in general agreement with these previous studies but showed that variations in *Lg Q* for the northeastern United States correlate roughly with large-scale tectonic features.

Discussion and Conclusions

Southern California and the Basin and Range Province of the western United States are well described by low *Lg Q* and a strong frequency dependence, while the eastern United States and southeastern Canada are best described by high *Lg Q* and weak frequency dependence (Fig. 16a). In addition, *Lg Q* displays a minimum between 0.5 and 1.0 Hz in the western United States, which is consistent with Aki

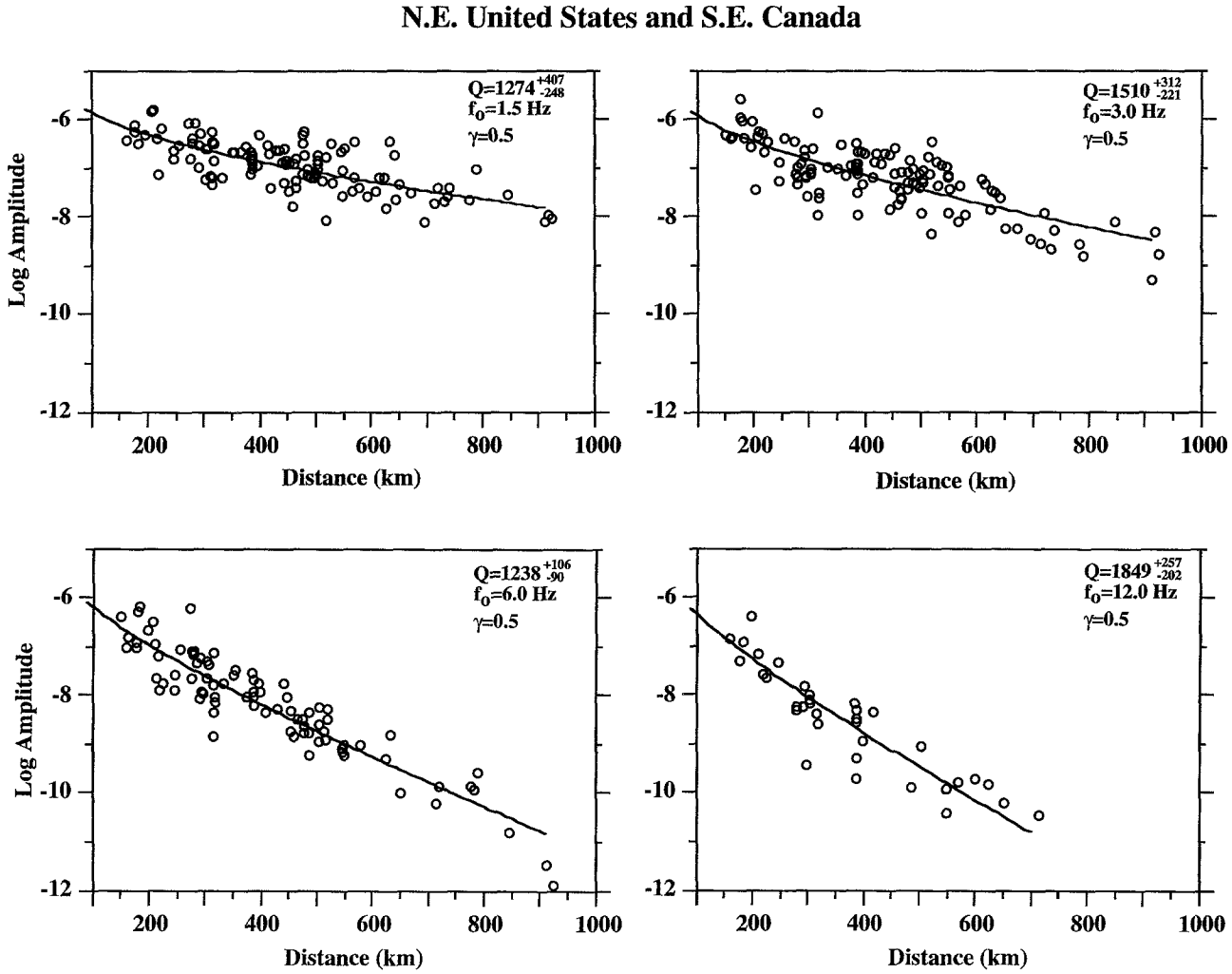

Figure 14. *Lg* spectral amplitudes (circles) for the northeastern United States and southeastern Canada at 1.5, 3.0, 6.0, and 12.0 Hz, corrected for source and receiver terms (see equation 3). The solid curve is the best-fit to the observed data assuming frequency-independent *Lg Q* and a γ of 0.5.

(1980) who proposed a minimum in lithospheric Q values near 1.0 Hz. Assuming that attenuation is due solely to scattering loss in a uniform random medium, Sato (1990) confirmed the conjecture of Aki (1980) that attenuation peaks near 1.0 Hz. A comparison of the *Lg* amplitudes and best-fit curves for each region at 6.0 Hz (Fig. 16b) shows clearly the significant decay of *Lg* amplitudes in the western United States study regions relative to the eastern study regions. In addition, a difference in amplitude decay with distance for southern California and the Basin and Range Province is noticeable, which is reflected in a different *Lg Q* function for the two regions. Differences in *Lg* attenuation between the central United States and the northeastern United States and southeastern Canada are not significantly different, which is reflected in similar *Lg Q* values at 6.0 Hz. *Lg* amplitudes (1.0 to 7.0 Hz; R = 150 to 700 km) in southern and south-central California are best-fit by the *Lg Q* function $Q = 187^{+7}_{-7}(f/1)^{0.55(\pm 0.03)}$, while *Lg* amplitudes over a comparable frequency range (1.0 to 5.0 Hz; R = 150 to 800 km) in the Basin and Range are fit by the *Lg Q* function $Q = 235^{+11}_{-11}(f/1)^{0.56(\pm 0.04)}$. Between 5.0 and 14.0 Hz, *Lg Q* in the Basin and Range Province is described by a change in frequency dependence with $Q = 575^{+11}_{-11}(f/5)^{1.05(\pm 0.09)}$. This change in frequency dependence is likely caused by contamination of the *Lg* phase by *Pn* and *Sn* phases at larger distances and high frequencies (Shin and Herrmann, 1987). The central United States is characterized by a frequency-independent *Lg Q* with a mean of 1291 (1.5 to 7.0 Hz; R = 150 to 900 km). Scatter in the *Lg Q* estimates and limited frequency range of observations preclude the determination of a possible frequency-dependent *Lg Q* for this region. For the northeastern United States and southeastern Canada, a frequency-dependent *Lg Q* of $1052^{+91}_{-83}(f/1.5)^{0.22(\pm 0.06)}$ (1.5 to 14.0 Hz; R = 150 to 900 km) is consistent with previous

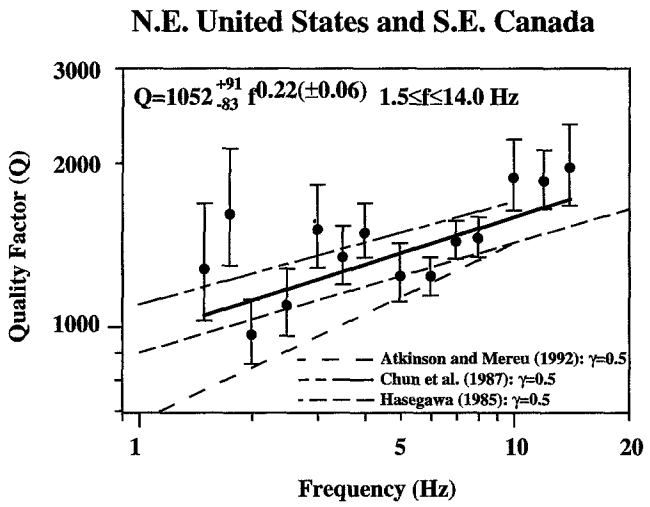

Figure 15. Values of Lg Q in the northeastern United States and southeastern Canada determined by inversion of the Lg spectral amplitudes measured every quarter-octave frequencies between 1.5 and 14.0 Hz, assuming frequency-independent Lg Q at each frequency and a γ of 0.5. Best-fit frequency-dependent Lg Q function is $Q = 1052^{+91}_{-83} f^{0.22(\pm 0.06)}$ between 1.5 and 14.0 Hz.

Lg attenuation studies for this region (Hasegawa, 1985; Chun *et al.*, 1987; Atkinson and Mereu, 1992).

In this article, our goal was to document differences in Lg attenuation between regions rather than to investigate the causes of differences and the frequency dependence. By using standardized instrumentation and consistent processing for each of the four study regions, this article provides attenuation functions that can be used in a variety of applications involving local earthquake monitoring and engineering studies.

Acknowledgments

We thank the Canadian National Seismograph Network and the data centers at UC-Berkeley and IRIS for providing the high-quality data used in this study. Gail Atkinson, Antonio Villasenor, Chuck Mueller, and an anonymous reviewer provided helpful comments on the manuscript. This research was partially supported by the Nuclear Regulatory Commission and the National Earthquake Hazards Reduction Program.

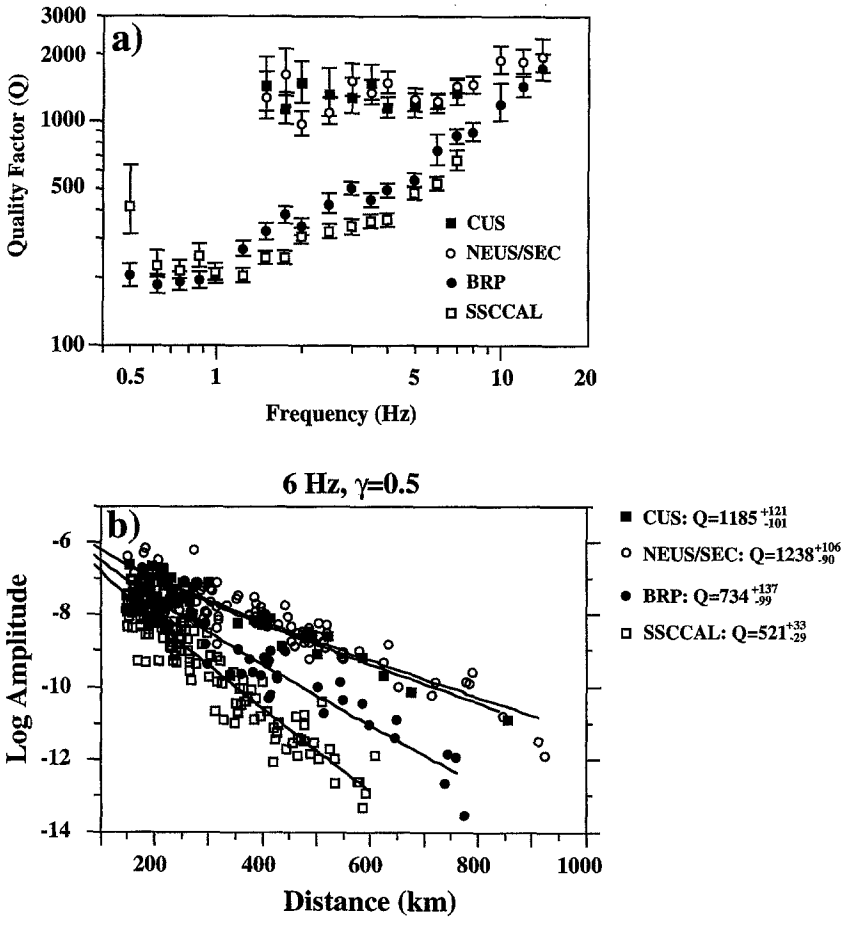

Figure 16. A comparison for each of the study regions of Lg Q as a function of (a) frequency and (b) Lg spectral amplitudes at 6.0 Hz, corrected for source and receiver terms. The solid curves in (b) are the best-fit to the observed data assuming frequency-independent Lg Q and a γ of 0.5. Key to symbols: open squares represent southern and south-central California (SSCCAL), filled circles represent the Basin and Range Province (BRP), filled squares represent the central United States (CUS), and filled circles represent the northeastern United States and southeastern Canada (NEUS/SEC).

References

Aki, K. (1980). Scattering and attenuation of shear waves in the lithosphere, *J. Geophys. Res.* **85,** 6496–6504.

Atkinson, G. M. and R. F. Mereu (1992). The shape of ground motion attenuation curves in southeastern Canada, *Bull. Seism. Soc. Am.* **82,** 2014–2031.

Boatwright, J. (1996). Attenuation of weak motion in the southern Great Basin, *Bull. Seism. Soc. Am.* **86,** 000–000.

Bowman, J. R. and B. L. N. Kennett (1991). Propagation of Lg waves in the northern Australian craton: influence of crustal velocity gradients, *Bull. Seism. Soc. Am.* **81,** 592–610.

Brockman, S. R. and G. A. Bollinger (1992). Q estimates along the Wasatch Front in Utah derived from Sg and Lg wave amplitudes, *Bull. Seism. Soc. Am.* **82,** 135–147.

Castro, R. R., J. G. Anderson, and S. K. Singh (1990). Site response, attenuation and source spectra of S waves along the Guerrero, Mexico, subduction zone, *Bull. Seism. Soc. Am.* **80,** 1481–1503.

Chavez, D. E. and K. F. Priestley (1986). Measurement of frequency dependent Lg attenuation in the Great Basin, *Geophys. Res. Lett.* **60,** 551–554.

Chun, K. Y., G. F. West, R. J. Kokoski, and C. Samson (1987). A novel technique for measuring Lg attenuation—Results from eastern Canada between 1 to 10 Hz, *Bull. Seism. Soc. Am.* **77,** 398–419.

Ebel, J. E. (1994). The ML(F) magnitude scale: A proposal for its use for northeastern North America, *Seism. Res. Lett.* **67,** 157–166.

Frankel, A. and L. Wennerberg (1987). Energy-flux model of seismic coda: separation of scattering and intrinsic attenuation, *Bull. Seism. Soc. Am.* **77,** 1223–1251.

Frankel, A. (1991). Mechanisms of seismic attenuation in the crust: scattering and anelasticity in New York State, South Africa, and southern California, *J. Geophys. Res.* **96,** 6269–6289.

Gregersen, S. (1984). Lg-wave propagation and crustal structure differences near Denmark and the North Sea, *Geophys. J. R. Astr. Soc.* **79,** 217–234.

Gupta, I. N. and K. L. McLaughlin (1987). Attenuation of ground motion in the eastern United States, *Bull. Seism. Soc. Am.* **77,** 366–383.

Hasegawa, H. (1985). Attenuation of Lg waves in the Canadian Shield, *Bull. Seism. Soc. Am.* **75,** 1569–1582.

Herrmann, R. and A. Kijko (1983). Modeling some empirical vertical component Lg relations, *Bull. Seism. Soc. Am.* **73,** 157–171.

Knopoff, L., F. Schwab, and E. Kausel (1973). Interpretation of Lg, *Geophys. J. R. Astr. Soc.* **33,** 389–404.

McNamara, D. E., T. J. Owens, and W. R. Walter (1996). Propagation characteristics across the Tibetan Plateau, *Bull. Seism. Soc. Am.* **86,** 457–469.

Nuttli, O. W. (1973). Seismic wave attenuation and magnitude relations for eastern North America, *J. Geophys. Res.* **78,** 876–885.

Nuttli, O. W., G. W. Bollinger, and D. W. Griffiths (1979). On the relation between modified mercalli intensity and body wave magnitude, *Bull. Seism. Soc. Am.* **69,** 893–910.

Nuttli, O. W. (1986). Yield estimates of Nevada Test Site explosions obtained from seismic Lg waves, *J. Geophys. Res.* **91,** 2137–2151.

Sato, H. (1990). Unified approach to amplitude attenuation and coda excitation in the randomly inhomogeneous lithosphere, *Pageoph* **132,** 1–29.

Shi, J., W. Kim, and P. G. Richards (1996). Variability of crustal attenuation in the northeastern United States from Lg waves, *J. Geophys. Res.* **101,** 25231–25242.

Shin, T. C. and R. B. Herrmann (1987). Lg attenuation and source studies using 1982 Miramichi data, *Bull. Seism. Soc. Am.* **77,** 384–397.

Singh, S. and R. B. Herrmann (1983). Regionalization of crustal coda Q in the continental United States, *J. Geophys. Res.* **88,** 527–538.

Xie, J. and B. J. Mitchell (1990). Attenuation of multiphase surface waves in the Basin and Range Province. Part I: Lg and Lg coda, *Geophys. J. Int.* **102,** 121–137.

U.S. Geological Survey
Box 25046 MS966
Denver, Colorado 80225
(H.M.B., A.F.)

U.S. Geological Survey
MS 977, 345 Middlefield Road
Menlo Park, California 94025
(D.M.B.)

Manuscript received 5 June 1996.